UR-1398
ER-40685-846
CDF/PUB/PLUG_UPGR/PUBLIC/2897

CDF END PLUG HADRON CALORIMETER UPGRADE: DESIGN, PRODUCTION AND QUALITY CONTROL RESULTS.

P.de Barbaro, A. Bodek, H.S. Budd, Q. Fan, T. Haelen, B.J. Kim, P. Koehn, K. Michaud, M. Olsson, M. Pillai, W.K. Sakumoto, E. Skup, R.C. Walker and B. Winer
University of Rochester, Rochester, NY 14627

M. Albrow, R. Andree, R. Bossert, S. Delchamps, R. Dixon, K. Ewald, J. Freeman, J. Grimson, J. Kerby, W. Koska, P.J. Limon, F. Nobrega, A.L. Simmons and J. Strait
Fermi National Accelerator Laboratory, Batavia, IL 60510

C. Bromberg, J. Huston, J.P. Mansour, R. Miller, R. Richards, and C. Yosef
Michigan State University, East Lansing, MI 48824

V. Barnes, M. Fahling, A. Laasanen, J. Ross, and Q. Shen
Purdue University, West Lafayette, IN 47907

T. Uchida and J. Suzuki
University of Tsukuba, Ibaraki, Japan

J. Iwai
Waseda University, Tokyo, Japan

SCAN-9501294
CERN LIBRARIES, GENEVA

Abstract

We present an overview of the CDF End Plug Upgrade Project. The structure of the upgraded calorimeter and the design of the optical readout system is discussed. We describe the production of scintillating tile/fiber multi-tile assemblies (megatiles) and present the quality control results of megatiles produced for the CDF End Plug Upgrade Hadron Calorimeter. The sample of megatiles presented in this analysis corresponds to approximately 16,500 individual tile/fiber assemblies. We discuss the quality control requirements and present the distributions of the quantities measured during the QC process. The various contributions to the tile-to-tile light yield variations are isolated and discussed.

I. Introduction

A detailed description of the design and construction of the upgraded CDF End Plug Hadron Calorimeter can be found in Ref. [1]. Technical details on construction of the Hadron multi-tile assemblies (megatiles) are described in Ref. [2]. Some of the earlier studies leading to the final design of the optical system for the Hadron calorimeter can be found in Ref. [3]. The results of the 1991 test beam studies of the End Plug prototype calorimeter are described in Ref. [4]. A scintillating tile/fiber system for the upgraded CDF Plug Electromagnetic Calorimeter, which will be located in front of the End Plug Hadron Calorimeter, is described in Ref. [5].

II. Motivation for the Upgrade

The CDF Collaboration has successfully completed Run Ia in August 1993, with 21 pb^{-1} of data recorded on tape. Run Ib has started in December 1993 with the goal of accumulating at least 100 pb^{-1} of data. Following a fixed target run in 1996/97 and a shutdown for the Main Injector construction in 1997/98, the Tevatron will be switched back to the collider mode in 1999 (Run II) with a goal of 1 fb^{-1} of integrated luminosity. The Tevatron Collider schedule is shown in Table 1.

Following the installation of the Main Injector, luminosity of the Tevatron will be increased. In order to reduce the probability of multiple interactions in a single bunch crossing, the number of proton and antiproton bunches in the Tevatron (6×6 through Run Ib) will be increased to 36×36 in Run II.

Table 2 shows the probability of two or more visible interactions in a single bunch crossing for various conditions of the beam luminosity and number of bunches. The peak

*submitted to the IEEE Transactions on Nuclear Science

Table 1: The Tevatron Collider Schedule. Luminosity, L of the Collider Runs is expressed in $cm^{-2}sec^{-1}$.

	1988 Run	Run Ia 1992/93	Run Ib 1994/5	Run II 1999 (?)
Deliv. L	9.6 pb^{-1}	30 pb^{-1}		
Int. L	4 pb^{-1}	21 pb^{-1}	100 pb^{-1}	1 fb^{-1}
Peak L	2×10^{30}	9×10^{30}	1.5×10^{31}	1×10^{32}
Bunches	6 × 6	6 × 6	6 × 6	36 × 36
Interval	3.5 μsec	3.5 μsec	3.5 μsec	396 nsec

Table 2: Number of average events per single bunch crossing, assuming a visible cross-section of 44 mbarns. Luminosity is expressed in $cm^{-2}sec^{-1}$. The probability of two or more events per bunch crossing is shown in brackets.

Lum.	6 × 6	36 × 36	96 × 96
10^{30}	0.15 (7.5%)	0.017 (1.3%)	0.006 (0.5%)
10^{31}	1.50 (58.0%)	0.17 (12.3%)	0.058 (4.7%)
10^{32}		1.74 (79.0%)	0.58 (40.0%)

luminosity in Run Ia reached $9.2\times10^{30}cm^{-2}sec^{-1}$ leading to the 60% probability of multiple interactions per bunch crossing. Following the upgrade to the injection linac energy from the original 200 MeV to 400 MeV, the luminosity in Run Ib has increased by $\approx$ 50%.

The operational condition for Run II (36 × 36 bunches) will result in the reduction of the time interval between bunch crossings from the present 3.5 μsec to 396 nsec with the possibility of further reduction of the bunch spacing down to 132 nsec. The present gas calorimetry system in the plug region ($2.4 < \eta < 3.5$) can not collect the charge signals in such a short time intervals. Therefore the CDF Collaboration has decided to replace the calorimeters in the end plug and the forward regions covering the angular region of $3.5^0 < \theta < 37^0$ ($1.1 < \eta < 3.5$) with a system with much faster response time.

III. Structure of the Upgraded End Plug Calorimeter

The experience of CDF with the central calorimeter has proven the excellent long term stability of the plastic scintillator-based calorimeter. This fact, together with the very fast response time of the scintillator, prompted the collaboration to select a plastic scintillator-absorber calorimeter for the upgraded end plugs.

In addition to the advantage of faster timing, the scintillator-absorber sandwich calorimeter is much denser due to its higher sampling media compared to the gas proportional tube system used in the present plug calorimeter. Using 23 layers of 4 mm scintillator and 4.5 mm lead plate clad with 0.5 mm stainless steel on both sides, the electromagnetic compartment (EM) will be 23 X_0 deep, compared with 18 X_0 depth of the present calorimeter. However, it will occupy only 60% of the physical depth occupied by the present system.

The increase in the density of the EM will also improve the hermeticity in the transition region between the central and end plug calorimeters. In the present configuration, the 37^0 region is one of the sources of the transverse energy and the missing transverse energy measurement degradation. Higher density of the EM calorimeter will also improve the hermeticity at the edges due to smaller Moliére radius reducing the electromagnetic shower leakage.

The existing steel structure, consisting of twenty steel plates, each 5 cm thick, with 1.9 cm gaps in between acts as the return path of the solenoidal flux. It will be preserved in order not to alter the magnetic field map of the tracking volume. Layers of 6 mm thick scintillator inserted into the steel gaps will replace the present proportional tube layers in the hadronic compartment (HAD). The gap created by the shorter EM depth will be utilized by two additional HAD layers with stainless steel plates.

The present steel structure will be extended from $\theta = 10^0$ to 3.5^0 ($2.4 < \eta < 3.5$). The extension will eliminate the undesirable transition to a separate forward calorimeter. A significant benefit of having a single calorimeter is that the forward muon toroid will be pushed up against the end plug wall. As a result the gap between the central muon detector, which presently extends up to $\theta = 40^0$ ($\eta = 1$) and the forward muon toroids, covering the region $\theta < 17^0$, will be almost eliminated. A sectional view of one quadrant of the Upgraded CDF End Plug Calorimeter is shown on Fig. 1.

The Shower Maximum Detector (SMD) will be instrumented with two layers of 5 mm wide scintillator strips placed at the fifth EM layer corresponding to $\approx 6\ X_0$. The strips will be oriented at an angle of $\theta = \pm 22.5^0$ with respect to the central line of each of $\Delta\phi = 45^0$ unit. The centroids of electromagnetic showers will be measured by the SMD to an accuracy of a few millimeters to check the matching with the incident charged track. Additionally, the measured shower profiles will be used to examine the electron candidates and to reject π^0 contribution to the direct photon signal.

The mechanical parameters of the Upgraded EM, HAD, and SMD are summarized in Table 3.

A. *Tile-Fiber Readout*

We have chosen to build the Upgraded End Plug EM and HAD as scintillator based sampling calorimeters employing the optical fiber readout technique. The basic structure of the calorimeter will be a lamination of scintillator plates segmented into "tiles", interleaved with absorber plates. The EM calorimeter has lead plates, while the HAD calorimeter has steel plates. The EM and HAD will be segmented into the same projective towers. The trans-

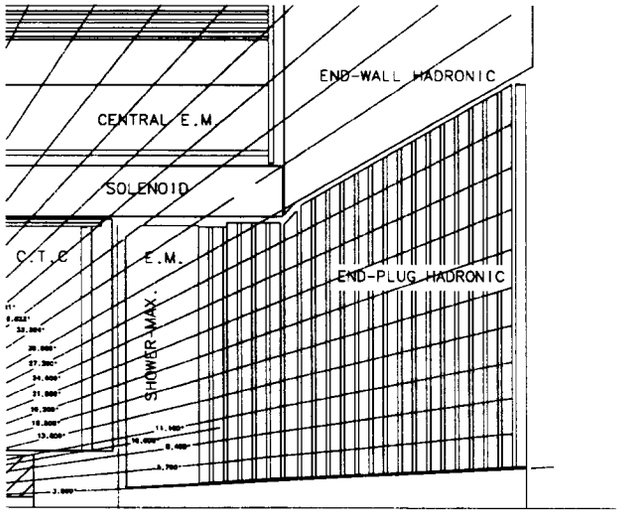

Figure 1: A sectional view of one quadrant of the Upgraded CDF End Plug Calorimeter. The EM compartment will cover pseudorapidity η region $1.1 < \eta < 3.5$ and the HAD compartment the region $1.3 < \eta < 3.5$.

verse segmentation of a 30^0 megatile is shown on Fig. 2.

The green wavelength-shifting (WLS) fibers [6] were imbedded in the scintillator tiles using the σ groove pattern [3]. The fibers for each 30^0 megatile are terminated at its radial edge using four connectors, carrying up to 9 fibers each. The optical cables, which are used to transport the light to the photomultipliers, are routed through the 2.5 cm gap between the central structure and the end plug to the rear of the calorimeter without sacrificing the hermeticity.

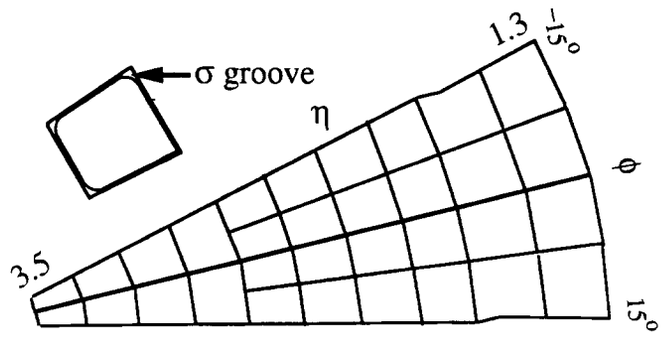

Figure 2: A transverse segmentation of a 30^0 megatile. Also shown is the σ pattern of the WLS fiber groove. As shown on Fig 1, the EM calorimeter and front layers of HAD have increased η coverage.

Table 3: Mechanical Parameters of the CDF Upgraded End Plug Calorimeter

EM	
Absorber	4.5 mm Pb
Cladding	0.5 mm S.S., on both sides
Scintillator	4 mm Polystyrene
Total depth	23 layers
Total thickness	35.7 cm (23.2 X_0, 0.96 λ_{int})
Sampling fraction	10.4%
Density	0.65 X_0/cm
Number of tiles	20448
Number of Towers	960
HAD	
Absorber	5.04 cm Fe
Scintillator	6 mm Polystyrene
Total depth	22 layers
Total thickness	160 cm (6.8 λ_{int})
Sampling fraction	2.03%
Number of tiles	16320
Number of Towers	864
Shower Max	
Scintillator	6 mm Polyvinyltoluene (PVT)
Total	2 layers
Number of Strips	6400

B. *Hadron Megatile Production*

In the subsequent sections, we concentrate on the description of the production and quality control process of megatiles for the Upgraded End Plug Hadron calorimeter. The production and quality control procedures of the EM and SMD were similar and are described elsewhere [1].

The production of Hadron megatiles consisted of several processes. Cutting of scintillator plates and machining of fiber grooves was done using the Thermwood computer controlled mill. Separation grooves between individual tiles were filled with a white paint/epoxy mixture to provide the optical isolation and mechanical strength of the megatiles. After the cutting and glueing operation, the megatiles were wrapped using white reflective paper (*Tyvek*) and light tightening material (*Tedlar*) and sandwiched between precut aluminum sheets. In a parallel process, fiber/connector assemblies were prepared and tested. Finally, the fibers were inserted into megatiles and the entire assembly underwent the quality control (QC) test.

IV. Quality Control Measurements

A. *UV Fiber Tests*

The optical WLS readout fibers were tested after they were mirrored, spliced to clear fibers, and assembled into mass-

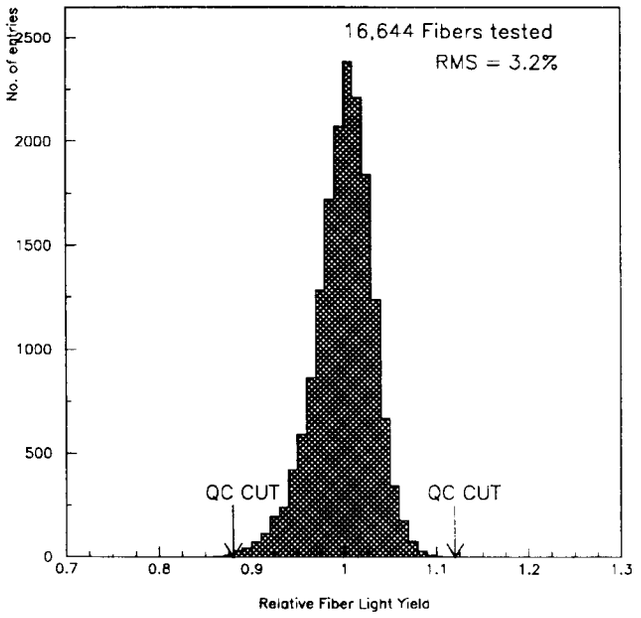

Figure 3: Distribution of the relative light yield of the optical fibers. The RMS of the fiber light yield is 3.2%. Fibers with relative light yield of less than 12% below the average were rejected.

terminated connectors. A total number of approximately 2600 fiber/connector assemblies was needed for the completion of the CDF End Plug Hadron Calorimeter project.

The fibers were tested by exciting them with an UV lamp and measuring their response using a photodiode/picoampmeter/PC setup [7]. The peak wavelength of the UV lamp used in the setup was 405 nanometers (nm). A blue filter was used to remove the harshest UV light of wavelength less than 385 nm. By measuring the light yield of individual fibers, we checked the quality of the polishing, reflectivity of the mirrors, the light transmission across the splice between wavelength shifter (WLS) and clear fibers, and the quality of the connector surface.

Figure 3 shows the distribution of the relative light yield of fibers as measured by the UV setup. The RMS of this distribution is 3.2%. The fiber light yield was normalized to the average light yield of the set of fibers with the same length. Fibers with relative light yield less than 12% below the average were rejected. During the production period discussed here, we have tested approximately 2000 fiber/connector assemblies containing over 16,500 fibers. In this sample, $\approx$ 0.7% of fibers were respliced and $\approx$ 2.5% of connectors were rejected.

The above described QC tests do not separately measure the light transmission across the WLS-to-clear fiber splice or the mirror reflectivity. In order to directly monitor these parameters special tests were periodically performed.

The light transmission across a splice can be best measured by studying the splices between two green WLS fibers. We first scanned a set of long green WLS fibers with no splices present. We then cut each fiber, polished the ends and spliced the fibers, keeping the cut fiber pairs matched. We then measured the ratio of light yields for these two scans and determined an average light yield transmission across the splice. The average light transmission across the splice of two WLS fibers is 92%, with the RMS of the distribution of $\approx$ 3%.

The fibers were aluminized in a bell jar system utilizing a magnetron sputtering gun driven by a DC power supply. For good reflectivity, we used 99.999% chemically pure (five nines) aluminum targets. The sputtering process was started after achieving a low 10^{-6} Torr vacuum, and then backfilling with "sputtering grade" Argon gas back up to 5 milliTorr (5 microns) pressure. The coating was approximately 2500 Angstroms thick and was monitored using an oscillating quartz crystal sensor device.

The mirror reflectivity was measured by a destructive test using fibers which were mirrored along with the fibers used for the Hadron megatile production. The fibers were first measured using the UV setup with the mirrored ends intact. The mirrored end of each fiber was then cut off and the light yield of fibers was measured again. In both of these measurements, the UV lamp was positioned near the mirrored end of the fibers. The ratio of these two light yield measurements was then used to determine the reflectivity of the mirror.

The average mirror reflectivity, was equal to 90% with an RMS of 5.4%. However, due to the attenuation of light in green WLS fibers, the typical increase of light yield of fibers with mirrored ends was $\approx$ 30 to 40%. Thus, the contribution to the variation of the fiber light yield originating from the variation in the mirror reflectivity was $\approx$ 1.5%.

B. *Collimated ^{137}Cs Source Test*

After passing the fiber QC test, the fibers/connector assemblies were inserted into the megatiles. The megatiles underwent the QC tests using a collimated ^{137}Cs γ source. We used a PC controlled motor system and data aquisition system to record the response of individual tiles to the radioactive source. The relative light yield of the tiles was measured using a set of photomultiplier tubes (PMT) for the readout and recording the DC current response.

To define the signal of each tile, we first correct the pedestal-subtracted signals (DC readings) for the PMT gain variation as measured by the response of a set of control tiles. We then define the relative light yield of a tile as its signal normalized to the average signal of all tiles from the same layer and tower.

Figure 4 shows the distribution of the relative tile light yield. The RMS of this distribution is 6.1%. Few tiles with relative light yield less than 22% below the mean were repaired. In such cases, we have either respliced its WLS fiber or replaced the entire fiber/connector assembly. The rejection rate of the connectors at this stage of QC process was $\approx$ 1.7%.

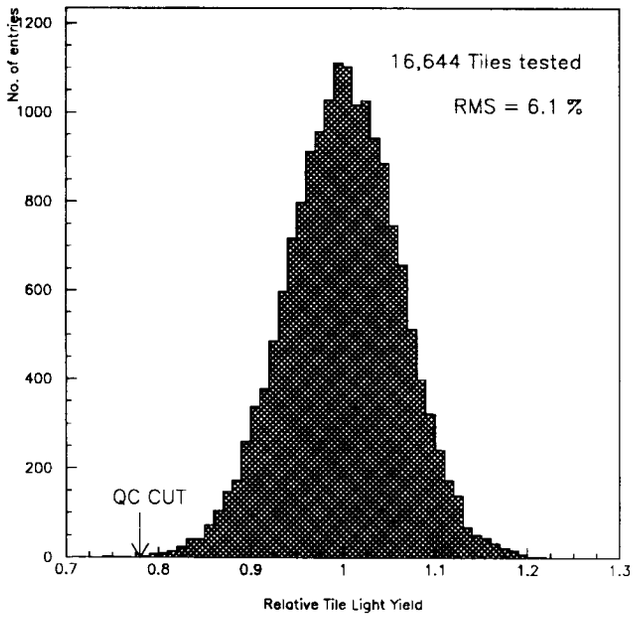

Figure 4: The distribution of the relative tile light yield. The RMS of the light yield is 6.1%.

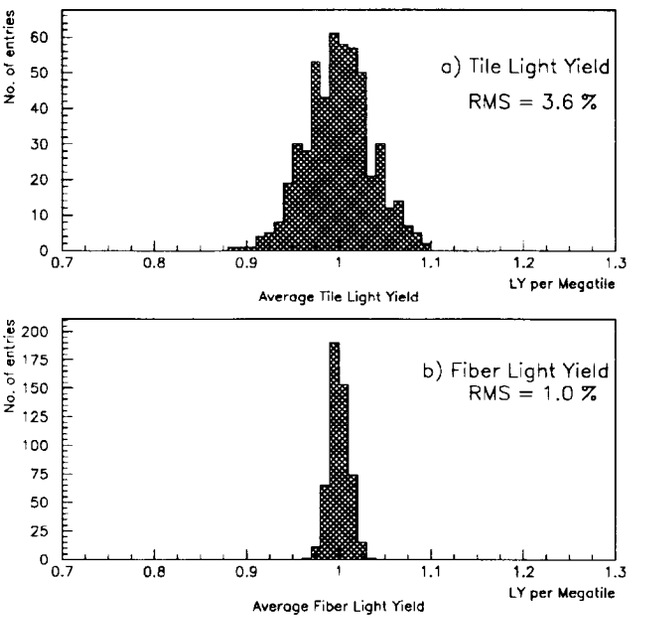

Figure 5: a) Distribution of the average megatile light yield, defined as the average relative light yield of all the tiles from a particular megatile. The RMS of this distribution is 3.6%.
b) Distribution of the average fiber light yield, defined as the average relative fiber light yield of all the fibers from a particular megatile. The RMS of this distribution is 1.0%

C. *Sources of Relative Light Yield Variation*

We define the total variation of the relative tile light yield distribution, σ_{tot}, as:

$$\sigma_{tot}^2 = \sigma_{fib}^2 + \sigma_{meg}^2 + \sigma_{other}^2 \qquad (1)$$

where σ_{fib} is the relative fiber light yield variation and σ_{meg} is the average megatile light yield variation. We define the average megatile light yield as an average relative light yield of all the individual tiles belonging to the same megatile. The σ_{meg} describes the additional contribution to the tile light yield variation due to systematic factors common to all tiles cut from the same scintillator plate.

The σ_{other} corresponds to the light yield variation due to other factors. These factors include the quality of optical coupling of fibers inside the megatile and local variations in the scintillator material thickness. It also includes possible damage to the fibers during the insertion into the scintillator or white plastic routing grooves. This contribution is presently under study.

As shown in Fig. 4, the total width of the relative light yield distribution of tiles, σ_{tot}, is 6.1%. We show below that the contributions to σ_{tot} originating from the fiber light yield variation (σ_{fib}) is 3.2%, contributions originating from the systematic megatile light yield variation (σ_{meg}) is 3.6%, and contributions due to other factors (σ_{other}) is 3.7%.

We can determine the systematic correlation in the light yield of tiles built from the same scintillator plate by studying the average megatile light yield. If there were no such correlations, the width of distribution of the average of 32 tiles in each megatile should be equal to $\approx$ 1.1% (from statistical arguments, we can calculate it by dividing the tile light yield RMS of 6.1% by $\sqrt{32}$). The distribution of the average megatile light yield for 510 measured megatiles has an RMS of 3.6%, (see Fig. 5a) significantly larger than 1.1%, indicating a systematic correlation in the light yield of tiles from same megatiles. However the distribution of the average fiber light yield (per each assembled megatile) has RMS of $\approx$ 1%, as shown of Fig 5b, only slightly above 0.6% expected for the fully uncorrelated distribution ($3.2\%/\sqrt{32}$).

The possible factors contributing to the variation of the average megatile light yield include the systematic variation in the thickness of scintillator plate and its absolute light yield, as well as the systematic variation in the quality of the grooves holding the WLS readout fibers.

The light yield of scintillator samples was determined using the position of the β source absorption peak and therefore its variation was not sensitive to the variation in the thickness of scintillator samples. Thus, the combined variation in the thickness of the scintillator plates (RMS equal to 1.2%) and the variation in the absolute light yield of scintillator (RMS equal to 1.6%) contributes 2% to σ_{meg}, the systematic variation in the light yield of tiles from same megatiles, equal to 3.6%.

Therefore we conclude, that there must be additional sources of the variation of average megatile light yield beyond variations in the average thickness and absolute light yield of scintillator plates. Certain processes, such as milling of fiber grooves, painting of tile edges with white paint or filling the separation grooves with white paint/epoxy mixture were performed at the same time for

all the tiles from same scintillator sheet. Systematic variations in the quality of these processes could therefore contribute to the increase of the σ_{meg}.

V. Front-to-Back Relative Light Yield Variation

In addition to studying the overall width (RMS) of the distribution of relative light yield of tiles, it is important to determine the average light yield of tiles as a function of the layer number. A systematic variation in light yield of tiles from the inner (front) layers relative to the outer (back) layers (sometimes referred to as front-to-back slope) could contribute to the degradation of the energy resolution of the calorimeter [9].

As described in the detail in Ref. [1], in order to minimize the front-to-back slope in the average response of tiles, during the design stage of the optical system of the calorimeter, we have adjusted the distance between the edges of tiles and the σ fiber groove inside the tile. In addition, the average light yield of tiles was adjusted by a suitable choice of the position of the WLS-to-clear fiber splices.

It is important to realize, that the tiles from various layers were tested using a same length optical cable (4 meters long), placed between the outer edge of the megatiles and the readout PMTs. However, in the future, following the installation of megatiles into the steel structure of the detector, the inner layers will be read out using longer clear optical cables than the outer layers.

In addition, the final light yield of tiles after installation in the B0 Hall, will be affected by the magnetic field present inside the calorimeter. The strength of magnetic field increases from negligible values for the outer most layers to 1.4 T for the inner most layers. Thus it increases the light yield of inner-most layers [10] by up to 10%.

Figure 6 shows the average light yield of tiles as a function of layer number. Layer 0 is the inner-most (front) layer, following the EM calorimeter, and layer 21 is the outer-most (back) layer of the Hadron calorimeter. The data was corrected for the two above described effects, the attenuation length of the clear optical cable and the effect of the magnetic field inside the hadron detector. As shown on the plot, the expected variation in the average light yield is within $\pm 10\%$ band. Our preliminary studies indicate [9] that this would not significantly contribute to the degradation of the energy resolution of the Hadron calorimeter.

VI. Wire source vs collimated source measurements

In addition to testing the megatiles with the collimated γ source, each megatile was scanned using an uncollimated γ source. In this case, the radioactive source was attached at

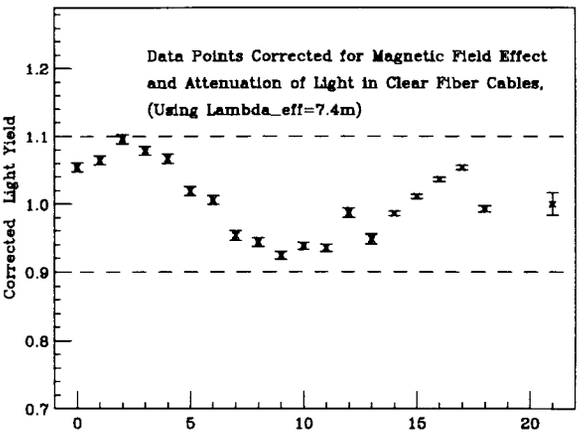

Figure 6: The relative tile light yield versus the calorimeter layer number. The data points were corrected for the effects of the magnetic field and attenuation length of the clear optical readout cable. The dashed lines at $\pm$ 10% around unity indicate the design goal for the variation of the average light yield of tiles.

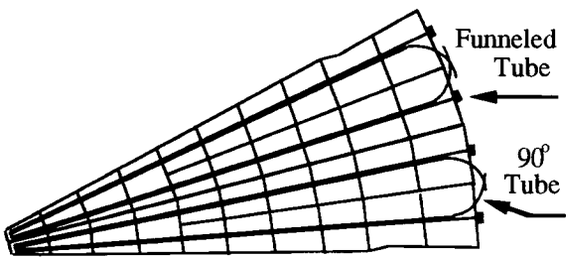

Figure 7: Positioning of wire source tube grooves for 30^0 megatiles. The funneled tubes are present in all megatiles. the 90^0 tubes were installed only in four selected layers.

the end of a wire which was inserted during the measurements into steel tubes embedded in each megatile. The steel tubes allowed us to guide the γ source over the geometrical center of individual tiles.

Positioning of source tubes is shown on Fig. 7. A set of tubes which are terminated at the radial edge of megatiles are only accessible when the plug is extracted. In addition, four selected layers of the Hadron calorimeter were equipped with tubes, bent at 90^0, to enable us monitoring of the response of scintillator tiles during the experiment.

The PMT signal was recorded as a function of position of the wire source inside the megatile. Individual tile responses were then determined using a peak-finding algorithm. The reproducibility of the peak finding procedure was determined by studying the ratio of tile response (see Fig. 8) as measured during the extension and the retraction of the wire source into the megatiles. The RMS of this distribution is 0.6%.

The wire source vs collimated source measurements allowed us to establish the calibration of the response of tiles to wire source. This calibration will be used in the future

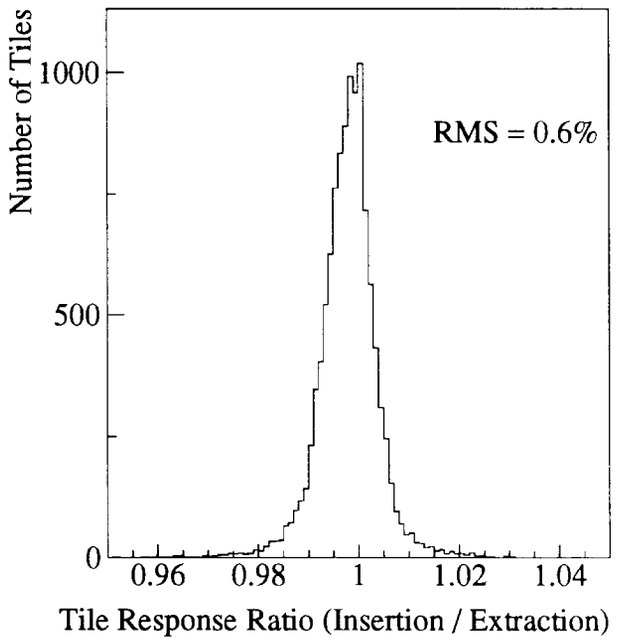

Figure 8: Ratio of tile response to the uncollimated γ source during the wire extensions and retractions. The RMS of this distribution is 0.6%.

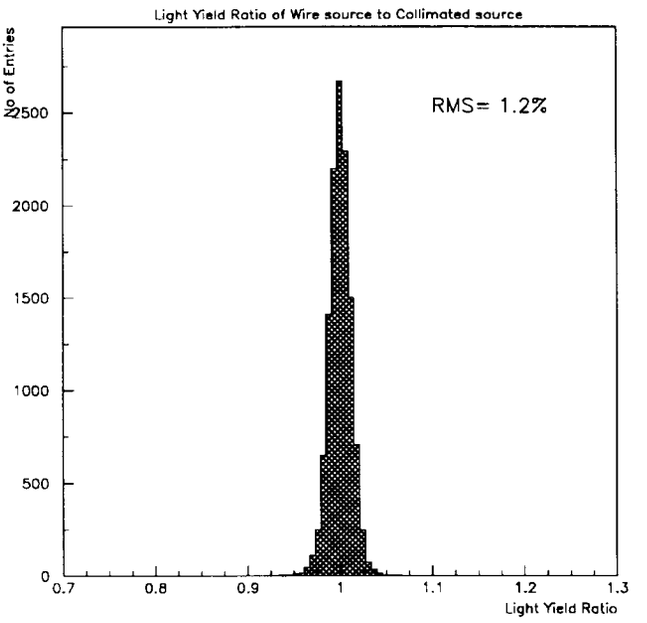

Figure 9: Distribution of the ratio of normalized wire source to the collimated γ source tile light yield, $R^{rel}_{w/c}$. The RMS of this distribution is 1.2%.

tests of the megatiles in the B0 Collision Hall after their assembly into the steel structure of the detector.

The ratio of wire source vs collimated source tile light yields, normalized separately for each layer and tower, $R^{rel}_{w/c}$ checked the positioning of the source tubes. The small RMS ($\approx$ 1.2%) of the ratio of the wire source to the collimated source light yield measurement (see Fig. 9) implied that the positioning of the steel tubes used to guide the wire source along the surface of megatiles was well controlled and did not introduce a large uncertainty to the wire source measurements.

VII. Optical Cross-talk between Adjacent Tiles

As mentioned earlier, individual tiles constituting a 30^0 megatile were joined together using a white paint/epoxy mixture [2]. Such procedure provided both, the mechanical strength of the assembly, as well as the optical isolation between the neighboring tiles. The cross-sectional view of a region between two neighboring tiles is shown in Fig. 10.

During the production, the separation grooves between the tiles were cut using a 0.035 inch (0.9 mm) diameter bit. The 6 mm thick scintillator plate was not cut entirely apart, leaving approximately 0.2 mm of uncut material below the separation groove. The uncut material, in addition to the backing material on the scintillator, allowed us to maintain the mechanical integrity of the entire megatile, until the separation grooves were filled with white paint/epoxy mixture.

However, the uncut scintillator material, approximately 3% of the total thickness of the scintillator plate, would introduce optical cross-talk between the neighboring tiles. We define the optical cross-talk between two neighboring tiles as the light yield of a particular tile when the source is placed on a neighboring tile normalized to the light yield with source placed on the center of the tile. Due to the finite size of the lead absorber used to collimate the γ source, a small amount of radiation from the source excited the neighboring tiles directly. This radiation cross-talk was determined to be between 0.7% to 0.9% and was subtracted from the total cross-talk measured between the neighboring tiles.

In order to suppress the optical cross-talk between neighboring tiles and reduce its sensitivity to the thickness of uncut material, we apply a permanent black marker line below the area of the separation groove. By absorbing the light, the black line reduced the optical cross-talk and made it much less sensitive to the thickness of uncut scintillator material.

The thickness of uncut scintillator in the separation groove varied between 0.15 to 0.3 mm, with the average equal to 0.2 mm. The optical cross-talk between individual tiles, as shown on Fig. 11 varied between 0 to 2%, with the average equal to $\approx$ 1%. Such values of optical cross-talk would not degrade the performance of the Hadron calorimeter.

VIII. Summary

We have measured the overall variation in the light yield of tiles used for the CDF Plug Upgrade Hadron calorimeter. The total width of this distribution (σ_{tot}) is 6.1%, with approximately 3.2% coming from the variation in the per-

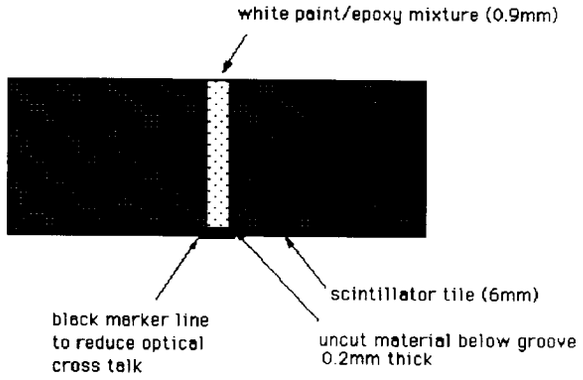

Figure 10: The cross-sectional view of the separation groove between two tiles. The black marker line applied below the separation groove, $\approx$ 2 mm wide, reduced the optical cross-talk between the neighbouring tiles to approximately 1%.

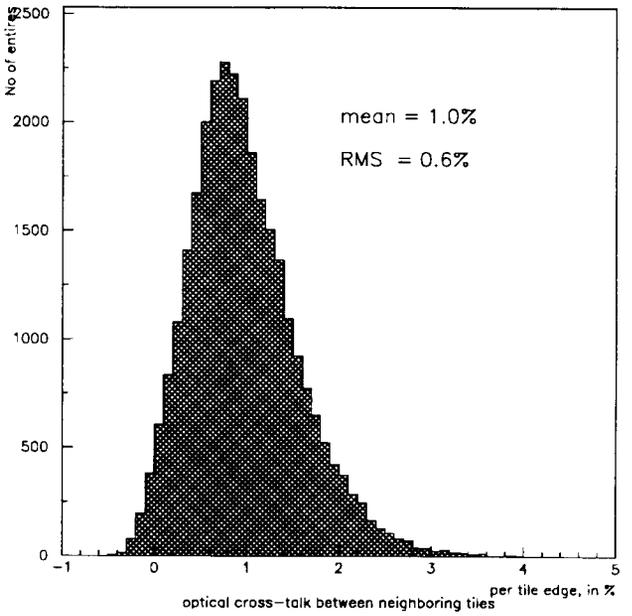

Figure 11: The distribution of the optical cross-talk between the neighboring tiles, as measured during QC tests of Hadron megatiles. The data has been corrected for the radiation cross-talk due to the finite size of the lead cone used to collimate the γ source.

formance of readout fibers (σ_{fib}), 3.6% from the systematic variation in light yield of tiles (σ_{meg}), and 3.7% due to other effects, such as tile/fiber optical coupling. The RMS of 6.1% is within the design goal of the End Plug Upgrade Hadron Calorimeter.

We have also studied the systematic variation in the average light yield of tiles from different layers of the Hadron calorimeter. The ratio is $\pm$ 10% within unity and meets the linearity design criteria of the calorimeter.

The optical cross-talk between neighboring tiles is below 2% and will not contribute to the degradation of the performance of the Hadron calorimeter. The QC studies also indicate that the wire sources can be used to calibrate the response of individual tiles with accuracy of $\approx$ 1.5%.

ACKNOWLEDGMENTS

We thank all of the Fermi Lab and university staff and technicians who worked on the Hadron calorimeter. We also acknowledge their support of the R&D effort leading to the design of the Hadron Plug Upgrade Calorimeter.

REFERENCES

[1] P. de Barbaro et al., *CDF Plug Upgrade Hadron Calorimeter Design*, U. of Rochester preprint UR-1360, May 1994.
Selected articles on Scintillator Tile-Fiber Calorimeters can be found in: *CDF End Plug Upgrade*, ed. by P. de Barbaro and A. Bodek, UR-1389, Oct. 1994.

[2] M. Olsson et al., *Techniques for Optical Isolation and Construction of Multi-Tile Assemblies in Scintillator Tile-Fiber Calorimeters Using White Epoxy*, UR-1370, Aug. 1994.

[3] P. de Barbaro et al., *R&D Results on Scintillating Tile/Fiber Calorimetry for the CDF and SDC detectors*, UR-1229, Sep. 1992, NIM **A315** (1992) 317.

[4] M.A. Lindgren, *The CDF Plug Calorimeter Upgrade*, in Proceedings of the Third ICCHEP, Corpus Christi, TX, Sep. 1992.

[5] S.Aota et al., *A Scintillating Tile/Fiber System for the CDF Plug Upgrade EM Calorimeter*, CDF Note 2431, Mar. 1994, to be published in **NIM**.

[6] Kuraray International Corp., 200 Park Ave., New York, NY 10166.

[7] J. P. Mansour et al., *A Semi-automated Splicer for Plastic Optical Fibers*, to be published in Proceedings of the 1993 Scintillating Fiber Workshop, Notre Dame, IN, Nov. 1993.

[8] V. Barnes et al., *Construction, Calibration and Characterization of an SDC Hadron Calorimeter Using a Moving Radioactive Source*, proc. of the Fifth ICCHEP, Brookhaven Nat. Lab., Sep. 1994.

[9] P. de Barbaro, A. Bodek and B. Winer, *The Effects of Tile Miscalibrations on the Performance of Tile/fiber based Hadron Calorimeter*, UR-1301, Jan. 1993.

[10] J.Mainusch et al., Nucl. Instr. & Meth. **A312** (1992) 451; D.Blömker et al., Nucl. Instr. & Meth. **A311** (1992) 505.